



Universiteit
Leiden
The Netherlands

Spin-momentum locking in oxide interfaces and in Weyl semimetals

Bovenzi, N.

Citation

Bovenzi, N. (2018, October 23). *Spin-momentum locking in oxide interfaces and in Weyl semimetals*. *Casimir PhD Series*. Retrieved from <https://hdl.handle.net/1887/66481>

Version: Not Applicable (or Unknown)

License: [Licence agreement concerning inclusion of doctoral thesis in the Institutional Repository of the University of Leiden](#)

Downloaded from: <https://hdl.handle.net/1887/66481>

Note: To cite this publication please use the final published version (if applicable).

Cover Page



Universiteit Leiden



The handle <http://hdl.handle.net/1887/66481> holds various files of this Leiden University dissertation.

Author: Bovenzi, N.

Title: Spin-momentum locking in oxide interfaces and in Weyl semimetals

Issue Date: 2018-10-23

1 Introduction

1.1 Preface

Spin-orbit coupling is a relativistic effect: A charged particle moving in an electric field experiences a magnetic field in a frame of reference in which it is at rest. This magnetic field acts on the spin magnetic moment, resulting in a coupling of the spin to the motion (the “orbit”). For massless particles the coupling reaches the extreme limit that the spin direction is tied to the direction of motion. One speaks of *spin-momentum locking*.

Since the discovery of graphene we have become familiar with the notion that conduction electrons can have a vanishing effective mass and thereby exhibit relativistic effects at velocities much smaller than the speed of light. In graphene spin-orbit coupling is very weak but the electrons have a sublattice degree of freedom (a “pseudo-spin”) that plays a similar role: it is oriented parallel to the momentum. Relativistic effects such as Klein tunneling emerge in graphene because of this pseudo-spin–momentum locking.

The topic of our thesis is to study the effects of spin-momentum locking in materials where it is the *real* spin, rather than a pseudo-spin, that is locked to the motion. We focus on two classes of materials: firstly on electrons confined to an oxide interface and secondly on the three-dimensional counterpart of graphene, known as a Weyl semimetal.

The remainder of this chapter is as follows. In Sec. 1.2 we introduce the topics of spin-orbit coupling and spin-momentum locking in condensed-matter systems. In Sec. 1.3 we discuss the electronic properties of interfaces in oxide heterostructures, with a focus on the high-mobility conducting system at the $\text{LaAlO}_3 / \text{SrTiO}_3$ interface and the investigation of its spin-orbit–driven physics through magnetotransport. In Sec. 1.4 the discussion shifts to Weyl semimetals, that offer the unique combination of gapless bulk spectrum, with relativistic energy–momentum relation, and topological surface states. For more accurate and self-contained treatments, references are provided throughout the text. We conclude with summaries of the following chapters.

1.2 Spin-orbit coupling and spin-momentum locking

The non-relativistic limit of the Dirac theory applied to atomic electrons leads to the Pauli Hamiltonian [1]

$$H_{SO} = -\frac{\hbar}{4m_0^2c^2}\boldsymbol{\sigma} \cdot \mathbf{p} \times \nabla V_0, \quad (1.1)$$

that encodes the interaction between the spin magnetic moment — represented by the vector of Pauli operators $\boldsymbol{\sigma} = (\sigma_x, \sigma_y, \sigma_z)$ — and the kinetic momentum \mathbf{p} of the electron. (V_0 is the electric potential of the atomic core, \hbar the reduced Planck’s constant, m_0 the bare electron mass and c the speed of light.)

In a solid crystal, electrons are subject to the periodic potential $V(\mathbf{r})$ of the ions’ lattice. The eigenfunctions of the one-particle Hamiltonian

$$H(\mathbf{r}) = -\frac{\hbar^2}{2m}\nabla^2 + V(\mathbf{r}) \quad (1.2)$$

are Bloch waves $\Psi_{n\mathbf{k}}(\mathbf{r}) = u_{n\mathbf{k}}(\mathbf{r})e^{i\mathbf{k}\cdot\mathbf{r}}$, where $u_{n\mathbf{k}}(\mathbf{r})$ is a periodic function with the periodicity of the lattice, and the eigenvalues $E_n(\mathbf{k})$ form bands as a function of the wave vector \mathbf{k} , labeled by the discrete index n .

The theory of electronic energy bands powerful tool that allows to classify “ordinary” materials in two big families: *insulators* and *metals*. The first ones have completely-filled (valence) bands that are separated by an energy gap from empty (conduction) bands, the second ones instead have partially-filled conduction bands. An insulator with a “small” gap between valence and conduction band can be made conducting via extrinsic doping, therefore it is called *semiconductor*. Semiconductors are the basic constituents of the electronic devices that we use in our daily life.

Spin-orbit coupling has remarkable effects on the band structure of semiconductors, such as splitting the spin-degeneracy of bands with finite angular momentum and enhancing — even by order of magnitudes — the Zeeman effect of an external magnetic field if the material lacks spatial-inversion symmetry [2].

Recently it has been realized that spin-orbit coupling can also lead to *topological* quantum states. For instance, due to large spin-orbit splitting in certain heavy-atom materials, valence and conduction bands are “inverted”. Although a finite gap remains for the bulk spectrum, conducting (gapless) states appear at energies within the bulk gap, that are localized at the boundaries of the system and robust against disorder [3–5]. A bulk insulator

1.2 Spin-orbit coupling and spin-momentum locking

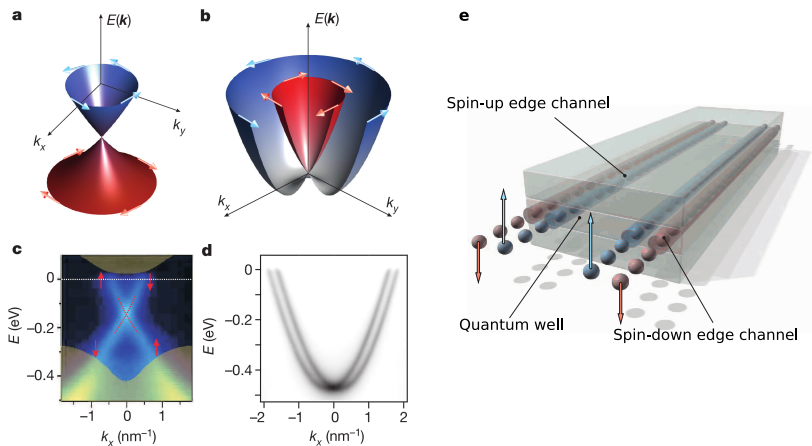


Figure 1.1: (a) Schematics of the helical spin structure of a Dirac cone at the surface of a three-dimensional topological insulator and (b) the chiral spin structure of two-dimensional parabolic bands with Rashba spin-orbit coupling. (c) ARPES measurements of the dispersion at the surface of the topological insulator $\text{Bi}_{2-x}\text{Ca}_x\text{Se}_3$ and (d) the surface of the normal metal Au(111) (plotted as a function of the momentum component k_x at a fixed k_y). Reprinted by permission from Springer Customer Service Centre GmbH: Springer Nature, Nature, A. Soumyanarayanan, N. Reyren, A. Fert and C. Panagopoulos, *Emergent phenomena induced by spin-orbit coupling at surfaces and interfaces*, Nature **539**, 509-517 (2016), Copyright 2016. Adapted by permission from Ref. 6, Nature Publishing Group. (e) Sketch of the conducting spin-polarized edge channels in a Quantum Spin Hall Insulator. From M. König, S. Wiedmann, C. Brüne, A. Roth, H. Buhmann, L. W. Molenkamp, X. L. Qi and S. C. Zhang, *Quantum Spin Hall Insulator State in HgTe Quantum Wells*, Science **318**, 766 (2007). Reprinted with permission from AAAS.

with conducting surfaces is topologically distinct from an ordinary insulator, thereby it is called *topological insulator*.

The combination of spin-orbit coupling and low-dimensionality, as e.g. at the surface of a topological insulator, gives rise to emergent physical effects in thin films and heterostructures [6]. The *Rashba effect* [7] at surfaces and interfaces describes the coupling between the inversion-symmetry-breaking electric field \mathbf{E} along the out-of-plane \mathbf{z} -direction and the spin magnetic moment of itinerant electrons. The Rashba Hamiltonian for s electrons (without orbital angular momentum) has the form

$$H_R = \alpha_R \hat{\mathbf{z}} \cdot (\mathbf{p} \times \boldsymbol{\sigma}), \quad (1.3)$$

where α_R is the coupling constant of the interaction, proportional to the electric field and to the intrinsic spin-orbit coupling.

In semiconductor-heterostructures, the magnitude of the Rashba effect can be electrically-modulated by means of external gates, that change

1 Introduction

the interface electric-potential and thereby the effective magnetic field [8]. This striking feature is at the basis of the spin field-effect transistor theoretically proposed by Datta and Das [9], where the strength of the spin-orbit coupling controls the rate of the spin-precession, and through that, the electrical current carried by electrons injected by a ferromagnetic contact into a gated semiconducting region and extracted at an opposite ferromagnetic contact.

The (spin) Rashba effect produces linear-in-momentum energy splitting of opposite-spin states and constrains the electron spin to lie in the direction perpendicular to the momentum. This is an example of “spin-momentum locking”, that can be generalized as a striking feature of surface (interface) states, such as:

- surface bands in ordinary metals [10],
- Dirac-cone states on the surfaces of three-dimensional topological insulators [11],
- edge channels in two-dimensional topological insulators (quantum spin Hall effect [12, 13]),
- Fermi-arc states in topological Weyl semimetals [14].

The basic picture of the Rashba effect becomes more complex when describing particles that have, in addition to the spin angular momentum, a finite orbital angular momentum, e.g. d electrons in oxide interfaces. In these systems, multiorbital effects produce a strong energy-dependence of the spin splitting and, at fixed energy, the magnitude of the splitting as a function of the momentum often deviates from linearity [15]. We can generalize the concept of spin-momentum locking in order to account for additional entanglement between spin and orbital polarizations.

1.3 Oxide interfaces

1.3.1 Transition-metal oxides

Transition metals are called the elements of the periodic table whose atoms either have an incomplete d subshell or can give rise to cations with an incomplete d subshell (IUPAC definition). They can form compounds with very different oxidation states: their oxide compounds (TMOs) show very interesting properties due to combination of the “hybrid” d electrons — partially bound to their own nuclei but with a certain freedom to interact

with neighboring atoms — and narrow electronic bands (between 1 and 2 eV) due to the small overlap between metal d orbitals and oxygen p orbitals. Hence, d electrons can show both itinerant and localized properties; the narrow band-width is expected to make electronic correlations relevant [16].

Two large subfamilies of the TMOs family are the *cuprates* and the *perovskites*. The former are famously known to show high-temperature superconductivity [17], the latter are among the most promising materials for highly efficient solar cells [18].

The perovskites have chemical formula AMO_3 and a cubic crystal structure, with the transition-metal (M) ion sitting at the center of the cubic cell, surrounded by an octahedron of oxygen (O) ions. and A ions at the eight corners. The crystal field generated by the O ions splits the five-fold degenerate d orbitals in two subsets, the lower-energy t_{2g} triplet (d_{xy}, d_{xz}, d_{yz} orbitals) and the higher-energy e_{2g} doublet ($d_{x^2-y^2}, d_{z^2}$).

Strontium titanate (SrTiO_3) has a long history as the *most dilute superconductor* — until the discovery of superconductivity in pure bismuth single crystals at ambient pressure and carrier density $n_e \approx 10^{15} \text{ cm}^{-3}$ [19] — with a transition temperature $T_c \approx 300 \text{ mK}$ [20]. Although a long history of studies, the nature of the electron-electron pairing mechanism in strontium titanate is still questioned [21]. Above T_c , the material is a band insulator with a gap of 3.2 eV and huge dielectric constant varying between $\epsilon_{\text{STO}} \approx 300$ at room temperature and $\epsilon_{\text{STO}} \approx 10000$ at sub-Kelvin temperatures [22].

Many TMOs have almost-matching lattice constants, whereby it is possible to grow layered heterostructures with atomic-size precision by placing one material on top of another layer by layer, using techniques developed in the context of semiconductor-heterostructures. Compared to the semiconducting counterparts, complex-oxide heterostructures are characterized by a richer mixing of different degrees of freedom — further enriched by the quantum confinement. Many oxide heterostructures are based on SrTiO_3 , due to its important dielectric properties.

1.3.2 The $\text{LaAlO}_3/\text{SrTiO}_3$ interface

A paradigmatic example of this class of materials is the heterostructure formed by growing a thin film of lanthanum aluminate (LaAlO_3) on a substrate of SrTiO_3 . Both materials are individually band-insulators. However, a breakthrough experiment reported evidence of electrical conductivity with high-mobility carriers at the interface of heterostructures grown along the (001) crystalline direction [23]. Since then, conducting

1 Introduction

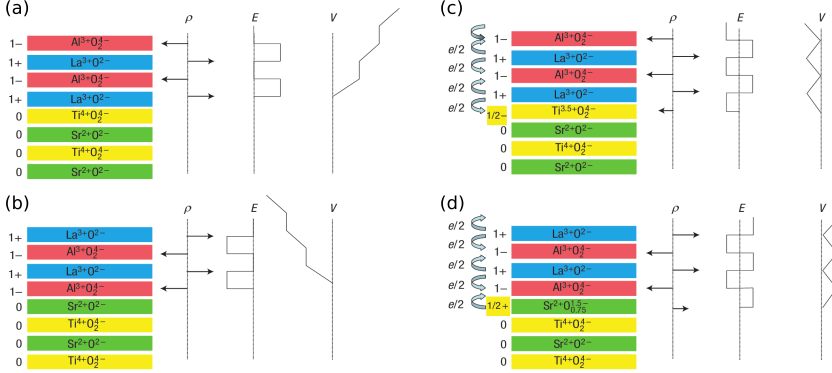


Figure 1.2: (001) LAO / STO heterostructures are made of electrically neutral planes on the STO side and charged planes on the LAO side. (a)–(b) Charge density ρ , electric field E and potential V along the growth direction at the unreconstructed interface with (a) TiO_2 -LaO connection and (b) SrO - AlO_2 connection. (c)–(d) Electronic reconstruction, with (c) half an electron per unit cell transferred to the TiO_2 interfacial plane and (d) half a hole transferred to the interfacial SrO plane, creates electric dipoles at the interface that leads to oscillating electric fields and bounded potentials. Reprinted by permission from Springer Customer Service Centre GmbH: Springer Nature, Nature Materials, N. Nakagawa, H. Y. Hwang and D. A. Muller, *Why some interfaces cannot be sharp*, Nat. Mater. **5**, 204–9 (2006), Copyright 2015.

interfaces were found in many SrTiO_3 -based heterostructures [21]. Nevertheless most of the (theoretical and experimental) research in the field has focused on the $\text{LaAlO}_3/\text{SrTiO}_3$ interface (henceforth, LAO/STO).

The (001) LAO / STO heterostructure is made of alternating AO and MO_2 planes — $\text{A}=\text{La}(\text{Sr})$ and $\text{M}=\text{Al}(\text{Ti})$. LAO planes are electrically polarized with alternating $\pm e$ charge (per two-dimensional unit cell), instead STO planes are neutral. Two types of interface are formed depending on the termination layer of the STO substrate: a n -type interface if the termination layer is TiO_2 (TiO_2 -LaO connectivity), a p -type interface in the case SrO - AlO_2 connectivity instead. The n -type interface becomes conducting when the thickness of the LAO film exceeds the threshold thickness of 3 unit cells, while the p -type interface does not show metallic behavior at any thickness [23, 24].

The origin of the interface conductivity is still debated. The *polar catastrophe* hypothesis [25] is consistent with many, but not all, the experimental observations. According to this hypothesis, a reconstruction of the electronic landscape of the interface occurs at a polar/non-polar junction in order to avoid the large cost in terms of electrostatic energy due to an unbounded growth of the electric potential in the bulk of the

polar material (see Fig. 1.2a–b).

The polar catastrophe mechanism predicts an insulator-metal transition (in n -type interfaces) as a function of the thickness of the LAO-film, when the bottom of the STO conduction band falls below the top of the LAO valence band, and charge-transfer is activated from the latter to the former. This prediction is consistent with the experiments. However, the electron density predicted by the polar catastrophe argument is much larger than the density of mobile electrons that is measured in transport [26, 27]. The discrepancy may be explained with the remaining electrons being bound at impurities or defects, thereby not contributing to the interface conductivity [28]. Moreover, conducting interfaces also exist in structures without polar discontinuity, as e.g. LAO / STO (110)–heterostructures [29].

Alternative proposals rely on the role played by oxygen-vacancies introduced in the system during the growth process [30–32].

1.3.3 Properties of the interface: superconductivity, magnetism, spin-orbit coupling

The huge STO dielectric constant allows to use electric gates to tune the charge-density of the interface between the fully-depleted regime and the overdoped regime with relatively low electric fields. The electric-field-dependence of physical properties such as spin-orbit coupling and superconductivity was experimentally reported [33, 34], that is a striking feature of the interface.

Regarding spin-orbit coupling, transport measurements clearly highlight the importance of it, although we are still waiting for ARPES (Angle Resolved Photo-Emission Spectroscopy) experiments that can resolve spin-split electronic bands. Signatures of weak-antilocalization peaks and their evolution as a function of the applied gate-voltage suggest that the magnitude of the spin-orbit coupling (spin-splitting) sharply increases of an order of magnitude at a doping level that seems to correlate with the appearance of superconductivity [35].

The density(voltage)-temperature phase diagram reveals a superconducting dome peaked at temperature $T_c^{max} \sim 300 \text{ mK}$ (very close to the critical temperature of bulk STO) and at a density in proximity of a Lifshitz transition [36], where the topology of the Fermi surface is altered by the appearance of additional bands. Contrary to the dome-structure of T_c , the magnitude of the superconducting gap measured (locally) via tunneling spectroscopy is found to increase both in the underdoped and in the overdoped regime [37], suggesting either the presence of a *pseudogap*

1 Introduction

phase like high- T_c superconductors [38] or that the system is spatially inhomogeneous, with coexisting superconducting and insulating (metallic) patches of nanometric size. In this scenario, patches with different densities would turn superconducting at slightly different temperatures, leading to a characteristic tail in the resistance-vs-temperature curves [39–41], unlike the usual sharp transition in homogeneous superconductors.

Signatures of inhomogeneous ground states of the interface appeared in magnetometry experiments [30, 42, 43] — that measured a ferromagnetic response superimposed to a diamagnetic (superconducting) signal. The inhomogeneity may be intrinsic, as the result of an electronic phase separation due to self-consistent adjustments of the confining potential that can make a homogeneous phase thermodynamically unstable [44]. However, alternative theoretical proposals pointed out that an exotic homogeneous phase that allows coexistence of superconductivity and magnetism, such as the FFLO (Fulde-Ferrel-Larkin-Ovchinnikov) phase [45], may be established in the system.

Interface superconductivity is a property inherited by the bulk STO parent compound. Instead, magnetism is an emergent property of the LAO / STO interface, since both LAO and STO are non-magnetic materials. Magnetic properties of the interface have been directly probed by means of many different techniques — Torque Magnetometry, SQUID Magnetometry, X-Ray Magnetic Circular Dichroism, Polarized Neutron Reflectometry, Magnetic Force Microscopy — and indirectly through magnetotransport measurements, with rather controversial outcomes. Even there are experiments that only measured finite magnetization at insulating interfaces and no signal in the conducting regime [46]. Many different groups have provided lots of magnetotransport whose interpretation is still subject of active research. A number of experimental signatures have been interpreted as originating from a Kondo-type interaction [47] between localized magnetic moments and delocalized electrons [48]:

- non-monotonic temperature-dependence of the sheet resistance [49];
- non-monotonic low-field Hall resistivity [36];
- giant negative magnetoresistance and crystalline anisotropy, with all-in-plane magnetic field [50];
- anomalous Hall effect [50].

However, the interaction-based interpretation of these observations was recently challenged by new experimental results obtained by Caviglia’s group at Delft University [51] for the case of in-plane magnetic field.

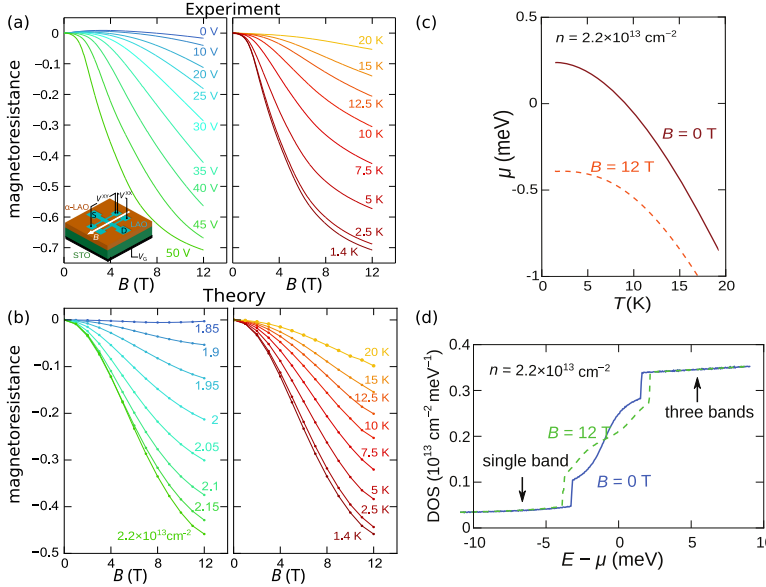


Figure 1.3: (a) Measured magnetoresistance of the LAO/STO interface, at temperature $T = 1.4$ K for several values of the gate voltage V_G (left panel) and at $V_G = 50$ V for various temperatures. (b) Magnetoresistance calculated within the semiclassical transport theory, at fixed temperature $T = 1.4$ K for various carrier-densities (left panel) and at density $n = 2.2 \times 10^{13} \text{ cm}^{-2}$ for various temperatures. (c) Temperature-dependence of the chemical potential μ and (d) density of states, calculated from the Hamiltonian 2.1 for an electron density $n = 2.2 \times 10^{13} \text{ cm}^{-2}$. Reprinted figures with permission from M. Diez, A. M. R. V. L. Monteiro, G. Mattoni, E. Cobanera, T. Hyart, E. Mulazimoglu, N. Bovenzi, C. W. J. Beenakker and A. D. Caviglia, *Giant negative magnetoresistance driven by spin-orbit coupling at the $\text{LaAlO}_3 / \text{SrTiO}_3$ interface*, Phys. Rev. Lett. **115**, 016803 (2015). Copyright (2015) by the American Physical Society.

Besides reporting a large negative magnetoresistance (up to 70% less than the zero-field resistance, in agreement with previous experiments), the experiments addressed the gate-voltage- and the temperature-dependence of the magnetoresistance, systematically, reporting that:

- the negative magnetoresistance survives up to ~ 20 K;
- the “critical” field, namely the value of the magnetic field where the slope of the magnetoresistance vs. field curves becomes negative, increases with the temperature;
- a striking similarity of the temperature-dependence (at fixed voltage) and the voltage-dependence (at fixed T) of the magnetoresistance.

1 Introduction

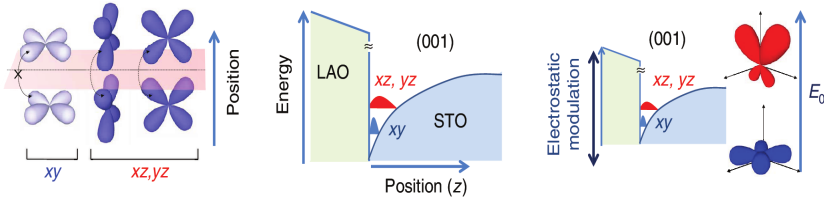


Figure 1.4: Confined orbitals in the quantum well at the (001) LAO / STO interface. Reprinted with permission from G. Herranz, G. Singh, N. Bergeal, A. Jouan, J. Lesueur, J. Gázquez, M. Varela, M. Scigaj, N. Dix, F. Sánchez and J. Fontcuberta, *Engineering two-dimensional superconductivity and Rashba spin-orbit coupling in LaAlO_3 / SrTiO_3 quantum wells by selective orbital occupancy*, Nat. Commun. **6**, 6028 (2015).

These observations required an alternative explanation, that is the subject of the theoretical work in Ref. 51. A semiclassical transport model for non-interacting electrons, that accounts for including multiorbital effects due to spin-orbit coupling and scattering by extended impurities, can qualitatively reproduce the features listed above. In particular, the striking similarity of temperature- and density-dependence of the magnetoresistance naturally arises from the renormalization of the chemical potential as a function of the temperature (see Fig. 1.3c).

Henceforth we refer to the mobile interface electrons as a two-dimensional electron gas (2DEG).

1.3.4 Band-structure model of the interface electron gas

Experiments report a dependence of the frequency of the conductance oscillations (Shubnikov-de Haas effect) only on the perpendicular component of the field [27, 52], as for a conventional two-dimensional electron gas. This means that the envelope wave function in the out-of-plane z -direction exists only in the lowest energy subband of the quantum well, although it can still extend over several unit cells away from the interface [53].

For the theoretical calculations of Chapter 2 we used the tight-binding model introduced in Ref. 48, that describes the conduction band of STO surface states. Restricting to the low-energy t_{2g} subspace, the Hamiltonian is calculated in the basis $|d_{xy}, \uparrow\rangle |d_{xy}, \downarrow\rangle |d_{xz}, \uparrow\rangle |d_{xz}, \downarrow\rangle |d_{yz}, \uparrow\rangle |d_{yz}, \downarrow\rangle$. The minimum of the band is at the Γ -point.

The orbital degeneracy of the bulk bands is partially removed due to the quantum confinement — d_{xy} orbitals have weak bonding along the out-of-plane direction — that results with the pair of d_{xy} bands, “light”

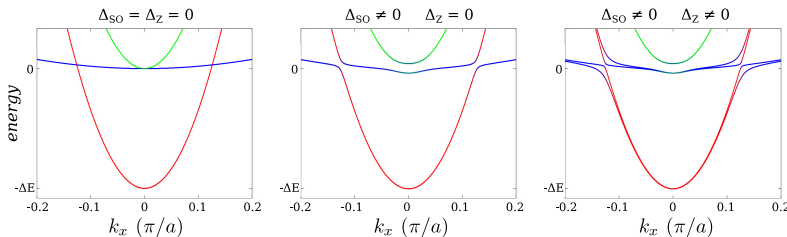


Figure 1.5: Band structures from diagonalization of the Hamiltonian 2.1, for three cases: only kinetic energy H_L ; with atomic spin-orbit coupling H_{SO} (center); with both atomic spin-orbit coupling and inversion-symmetry breaking H_Z (right).

(small effective mass) and isotropic, having lower energy than d_{xz} / d_{yz} bands, that are “light” in one in-plane direction and “heavy” in the other one.

The intrinsic spin-orbit coupling, inherited from the atomic orbitals, is an off-diagonal matrix in this basis, thereby it mixes spin and orbital polarizations. The main effects on the band structure are to remove the remaining orbital degeneracy between d_{xz} and d_{yz} states at the Γ point and to produce hybridized d_{xy}/d_{xz} (d_{yz}) states, opening gaps in correspondence of band-crossing points.

Finally, hopping elements between orbitals with different parity under $(x, y, z) \rightarrow (x, y, -z)$ transformation are non-zero in the absence of inversion symmetry [54]. These are next-nearest-neighbor spin-preserving processes between the even d_{xy} orbitals and the odd d_{xz}/d_{yz} orbitals.

In combination with the intrinsic spin-orbit coupling, this term produces a strongly energy-dependent spin-splitting, that abruptly increases near the hybridization gaps. More details about the Hamiltonian and the band structure are provided in Sec. 2.7 of Chapter 2.

1.4 Weyl Semimetals

1.4.1 Weyl fermions in crystals

Accidental degeneracies in the band structure of three-dimensional solids — where low-energy excitations have linear energy-momentum relation — are not rare [55]. However these degeneracies are lifted by any weak perturbation unless they are enforced by symmetry constraints or by the so-called “topological invariants” of the band structure.

1 Introduction

Symmetry-protected Dirac points exist both in two-dimensional (e.g. graphene) and in three-dimensional systems. Instead, the topologically-protected Weyl points are a unique property of three-dimensional crystals.

Each Weyl point (node) is a monopole of Berry curvature (a sort of momentum-space analog of the magnetic field) with a charge $\chi = \pm 1$ depending on the flux enclosed by a sphere surrounding the point. The sign determines the *chirality* (the “handedness”) of the Weyl-fermion’s wave function in real space.

Chiral fermions must always occur in pairs of opposite chirality according to the Nielsen-Ninomiya theorem [56] – in other words, the total Berry flux across the Brillouin zone must vanish. The low-energy physics around the Weyl point with chirality $\chi = \pm 1$ is governed by the Weyl Hamiltonian [57], that in momentum representation is

$$H_W = \chi v_F (p_x \sigma_x + p_y \sigma_y + p_z \sigma_z), \quad (1.4)$$

where $\sigma_{\alpha (\alpha=x,y,z)}$ are Pauli matrices and p_{α} the components of the crystal momentum $\mathbf{p} = \hbar \mathbf{k}$. The low-energy excitations have isotropic conical dispersion, with velocity v_F and the spin parallel or antiparallel to the momentum. Although Eq. (1.4) looks just like a trivial generalization of the two-dimensional graphene Hamiltonian, the third dimension enables topological protection to the band-touching points. Weyl cones cannot be gapped by local perturbations, as the only effect of adding a mass term $m\sigma_{\alpha}$ to H_W is of moving the Weyl cones around the Brillouin zone. The only way to make chiral fermions disappear is to pair them up, merging Weyl cones with opposite chirality that lead to the creation of a gap in the energy spectrum.

In order to acquire topological protection against local perturbations, a Weyl semimetal must not be invariant under the product of time-reversal and inversion symmetry. (If both symmetries are present, the Berry curvature is identically zero at any \mathbf{k} -point).

More “flavors” of Weyl fermions can exist in the band-structure of three-dimensional crystals, where the effective low-energy theory is not constrained by Lorentz invariance, that instead forces the energy-momentum relation of a fundamental particle to be independent of the direction where the particle travels. Therefore, Weyl cones are often anisotropic and tilted — the tilting is realized by adding the term $\propto p_{\alpha} \sigma_0$ to the Weyl Hamiltonian. In some materials the distortion can be so strong that it tips the cone over the momentum axis p_{α} , realizing a topologically distinct class of protected band touchings, the type-II Weyl points. These protected crossing points connect electron-like and hole-like states coexisting at the energy of the Weyl point [58].

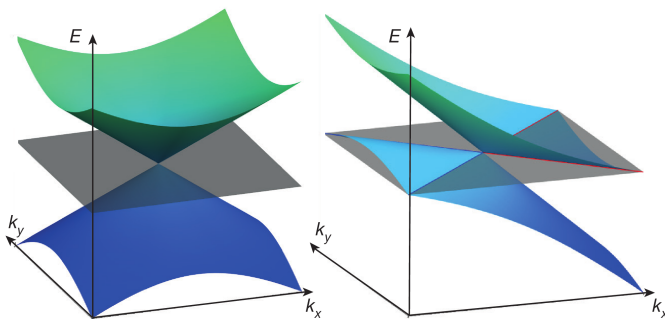


Figure 1.6: Type-I (left) and type-II (right) Weyl cones as a function of the momentum components k_x, k_y (at $k_z = 0$). The type-II Weyl cone has finite density of states at the energy of the Weyl node. Up to linear terms in the energy-momentum dispersion the equi-energy contours near the Weyl-node energy are open. On a lattice, higher-order terms close the contours. Reprinted by permission from Springer Customer Service Centre GmbH: Springer Nature, Nature, A. A. Soluyanov, D. Gresch, Z. Wang, Q.S. Wu, M. Troyer *et al.*, *Type-II Weyl semimetals*, Nature **527**, 495-98 (2015), Copyright 2015.

Furthermore, combinations of point-group symmetries of the crystal structure [59] can force more Weyl points with same chirality to merge, producing Berry monopoles with topological charge larger than one. These are called “multi-Weyl” points. Type-II and multi-Weyl points are studied in Chapter 5.

1.4.2 Lattice model of time-reversal-symmetry breaking Weyl semimetals

For lattice simulations, we use the tight-binding model of a time-reversal-symmetry breaking Weyl semimetal on a cubic lattice (with lattice parameter $a \equiv 1$) introduced in Ref.132, defined by the Hamiltonian

$$H_W(\mathbf{k}) = \tau_z(\sigma_x t_x \sin k_x + \sigma_y t_y \sin k_y + \sigma_z t_z \sin k_z) + m_{\mathbf{k}} \tau_x \sigma_0 + \beta \tau_0 \sigma_z + \lambda \tau_z \sigma_0 - \mu_W \tau_0 \sigma_0, \quad (1.5a)$$

$$m_{\mathbf{k}} = m_0 + t'_x(1 - \cos k_x) + t'_y(1 - \cos k_y) + t'_z(1 - \cos k_z). \quad (1.5b)$$

The σ and τ Pauli matrices refer to a spin and orbital degree of freedom, σ_0 (τ_0) is the 2×2 identity matrix in spin (orbital) space. t_α and t'_α are respectively kinetic hopping and spin-dependent hopping terms —

1 Introduction

originating from spin-orbit coupling. The mass term $m_{\mathbf{k}}$ ensures that the spectrum is gapped everywhere except at $\mathbf{k} = (0, 0, \pm K)$, with

$$K^2 \approx \frac{\beta^2 - m_0^2}{t_z^2 + t'_z m_0} \quad (1.6)$$

where the origins of two Weyl cones with opposite chirality are located. β (λ) is the parameter that breaks time-reversal (inversion) symmetry providing a difference in momentum (energy) of the two Weyl points.

The Hamiltonian 1.5a is mathematically equivalent — up to a unitary transformation and redefinition of the τ degree of freedom — to the model of Ref. 63, where Weyl fermions are engineered in the phase diagram of a multilayer heterostructure realized by alternating layers of a magnetically doped topological insulator (such as Bi_2Se_3) and normal-insulator layers. Although experimentally very challenging, the latter model is fascinating also because by replacing the normal-insulator layers with thin films of s -wave superconductor, it is predicted to realize a *Weyl superconductor* [60]. We make use of the heterostructure models in Chapter 3 in the context of Andreev reflection in Weyl superconductor – Weyl semimetal junctions.

1.4.3 Surface states

A closed system whose bulk band structure exhibits Weyl fermions is further characterized by a special type of surface states. To understand how the surface states arise, let us consider two Weyl cones centered at momenta $\chi\mathbf{k}_0 = (\chi k_0, 0, 0)$ and let us slice the 3D Brillouin zone in a series of planes, parametrized by the momentum component k_x . To each plane corresponds a two-dimensional band structure that has a gap for all values of k_x except for $k_x = \pm k_0$. A Chern number is associated to each gapped band structure as:

$$C_{k_x} = \frac{1}{2\pi} \int_{S_{k_x}} d\mathbf{S}_{k_x} \cdot \boldsymbol{\Omega}_{\mathbf{k}} \quad (1.7)$$

with

$$\boldsymbol{\Omega}_{\mathbf{k}} = \nabla_{\mathbf{k}} \times \mathbf{A}_{\mathbf{k}} \quad \mathbf{A}_{\mathbf{k}} = \sum_n i \langle u_{n\mathbf{k}} | \nabla_{\mathbf{k}} | u_{n\mathbf{k}} \rangle, \quad (1.8)$$

where $\mathbf{A}_{\mathbf{k}}$ is the Berry potential summed over all filled bands labeled by the index n and $u_{n\mathbf{k}}$ are Bloch states.

By tuning the parameter k_x continuously, the system undergoes a topological phase transition with gap closing and reopening across a Weyl point, that is accompanied by a change of the Chern number of the planes. Planes with $|k_x| < k_0$ carry non-zero Chern numbers, hence they support

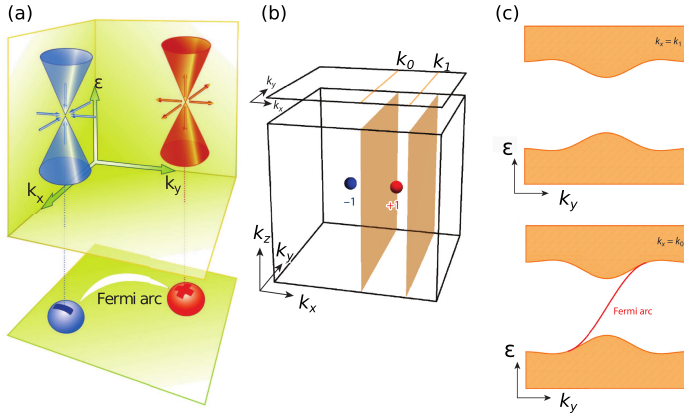


Figure 1.7: (a) Pair of opposite-chirality Weyl cones in the three-dimensional Brillouin zone. (b) Graphic argument for the development of the Fermi arcs from connecting edge states of the Chern insulators defined by the band structure on two-dimensional slices of the Brillouin zone in between the Weyl nodes. (c) At $k_x = k_1$ (top) the effective two-dimensional Hamiltonian describes a trivial insulator (Chern number $\nu = 0$) with a gapped bulk spectrum and no edge states. At $k_x = k_0$ (bottom) instead the band structure has non-trivial Chern number $\nu = \pm 1$, that corresponds to the presence of one edge state within the bulk gap. Adapted from Ref. [14].

chiral states propagating along the edges. The surface bands appear on the two-dimensional surface by joining together edge states supported by the non-trivial planes in-between the Weyl points. The intersection of the surface bands with the Fermi energy generates open curves that connect the projections of the Weyl points onto the surface Brillouin zone, that are called “Fermi arcs”.

In real space, the surface states are “chiral”, meaning that they circle around the magnetization axis in a single direction. If inversion symmetry is broken they acquire finite velocity along the magnetization axis; in cylinder geometry with the Weyl points along the axis of the cylinder, the surface states form a solenoid structure [61].

However, Fermi arcs on opposite material’s surfaces must be thought as complementary parts of a single Fermi surface. Indeed, in thin-film Weyl semimetals arcs on top and bottom surfaces merge to form a closed equi-energy contour. Interestingly, when both time-reversal and inversion symmetry are broken in a Weyl thin-film, the intersection of the constant energy planes with the lowest energy subband produces a figure-8, that is topologically distinct from simple deformations of the Fermi circle in conventional 2DEGs. Magnetotransport signatures of this Fermi surface

1 Introduction

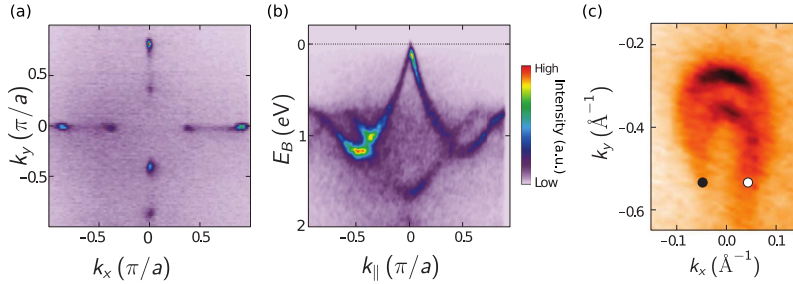


Figure 1.8: (a) ARPES-measured dispersion on the surface Brillouin zone and (b) in the bulk of the recently discovered TaAs Weyl semimetal. (c) High-resolution image of two Fermi arcs terminating at the projections of opposite-chirality Weyl nodes. From S.-Y. Xu, I. Belopolski, N. Alidoust, M. Neupane, G. Bian, *et al.*, *Discovery of a Weyl fermion semimetal and topological Fermi arcs*, *Science* **349**, 613 (2015). Reprinted with permission from AAAS.

are investigated in Chapter 4.

1.4.4 Experimental realizations

The search for a Weyl-semimetal phase initially focused on inversion-symmetric systems with broken time-reversal symmetry. Early proposals suggested magnetic pyrochlore iridates [62], multilayer heterostructures of alternating magnetically doped topological insulators and normal insulators [63], magnetically doped topological insulators at the critical point of transition to a normal insulator [64]. Moreover the recently discovered Dirac semimetals [65–67] — where the band-touching point is at least four-fold degenerate due to crystalline symmetries — can be turned to a Weyl semimetal by splitting a single Dirac point into two Weyl points with a Zeeman field. All these proposals suffer a number of experimental challenges that prevented the realization of any of them to date.

Meanwhile, time-reversal-invariant Weyl semimetals have been brought to life: first in tantalum arsenide (TaAs), later in niobium arsenide (NbAs) and tantalum phosphide (TaP) [68] — all these materials break inversion symmetry and have 24 Weyl cones in the Brillouin zone — the bulk conical dispersion and the surface Fermi arcs were resolved with good resolution in ARPES experiments.

Transport signatures of a magnetic Weyl semimetal were identified in different topological Heusler compounds [69, 70] and, very recently, evidences for a magnetic Weyl semimetal have been reported in photoemission

data from the correlated manganese-tin alloy (Mn_3Sn) [71], an hexagonal antiferromagnet with a stacked Kagome lattice.

1.4.5 Chiral anomaly and related magnetotransport signatures

Weyl fermions in condensed-matter systems are predicted to show the *chiral anomaly* [72, 73] — the non-conservation of the currents carried by the individual chiral species in the presence of parallel electric and magnetic field [74]. The anomaly manifests itself as the pumping of chiral electrons between oppositely charged Weyl points, leading to “valley” polarization. The anomaly is a general feature of chiral fermions in odd spatial dimensions. Its simplest one-dimensional version only requires an electric field, whose action on the electron dynamics is given by the semiclassical equation of motion $dk/dt = eE/\hbar$. If right-moving and left-moving carriers are connected at high energies (as is the case of any realistic band-structure), change of momentum implies transferring electrons from the left-moving to the right-moving Weyl point. As a result the difference between the densities of left and right movers n_L and n_R grows according to

$$\frac{d(n_R - n_L)}{dt} = 2\frac{e}{h}E. \quad (1.9)$$

This is the chiral anomaly in one-dimensional systems. The right-hand-side of Eq. (1.9) will have an additional term that oppose to the growth of the left-hand-side if the density imbalance can be relaxed via inter-node scattering. In the three-dimensional space, the quantizing effect of the magnetic field is necessary to recover an effective one-dimensional transport problem. Indeed an external magnetic field produces Landau levels that disperse only in the direction of the field. The Landau level with quantum number $n = 0$ in a Weyl semimetal is chiral, namely it has velocity parallel or antiparallel to field-direction, depending on the chirality of the Weyl node from where it is generated. If an electric field is applied parallel to the magnetic field, electrons start propagating along one-dimensional chiral channels, that have cross-sectional area (divided by the number of the degenerate states) $\mathcal{A} = \phi_0/B$, the ratio between the flux quantum and the magnetic field. Therefore, formula 1.9 holds, upon substituting E with $\mathbf{E} \cdot \hat{\mathbf{B}}$ and dividing by the cross sectional area \mathcal{A} to obtain the three-dimensional density. Although no current in equilibrium is allowed, in a non-equilibrium setup the chiral anomaly result in a contribution to the total electrical current of a Weyl semimetal that leads to the longitudinal

negative magnetoresistance [75–77] and the chiral magnetic effect with and without Landau levels [78, 79].

1.5 This thesis

1.5.1 Chapter 2

The study of magnetotransport effects, in connection with spin-orbit coupling, at the LAO /STO interface requires more theoretical efforts that may help interpret the experiments. The work presented in this chapter extends the results of Ref. [51]. Here we address — by applying the semiclassical transport theory to spin-coupled electrons scattered by extended impurities on the plane of the interface — the anisotropy of the longitudinal magnetoresistance under in-plane magnetic fields, that was reported by several experimental groups in recent years, but not reproduced by any theoretical model so far.

We calculate the full resistivity tensor as a function of the orientation of the in-plane field, for different values of the field-strength and several electron densities. The results show that the high-field angular-modulation of the magnetoresistance has a behavior similar to what observed in the experiments: because of the peculiar spin-orbital-momentum locking of the states at the Fermi level, the largest contributions to the resistance come from *inter-band* scattering processes, that are extremely sensitive to the applied magnetic field. Finally, we show that a sizable Hall resistivity is possible even in the absence of an orbital magnetic field and/or magnetic impurities. Unlike the longitudinal magnetoresistance, the Hall signal is due to *intra-band* scattering processes. We also comment on the differences with respect to the experiments.

1.5.2 Chapter 3

A Weyl semimetal with broken time-reversal symmetry (*magnetic Weyl semimetal*) has a minimum of two species of Weyl fermions, distinguished by their opposite chirality. Therefore, a hydrogen-atom model of the band structure of a (unbounded) magnetic Weyl semimetal consists of a pair of Weyl cones at opposite momenta $\pm K$ that are displaced in the direction of the internal magnetization. In the presence of inversion symmetry, the (pseudo)spin degree of freedom of a Weyl fermion with positive (negative) chirality is tied parallel (antiparallel) to its kinetic momentum.

At a normal-metal/superconductor junction, an electron injected from

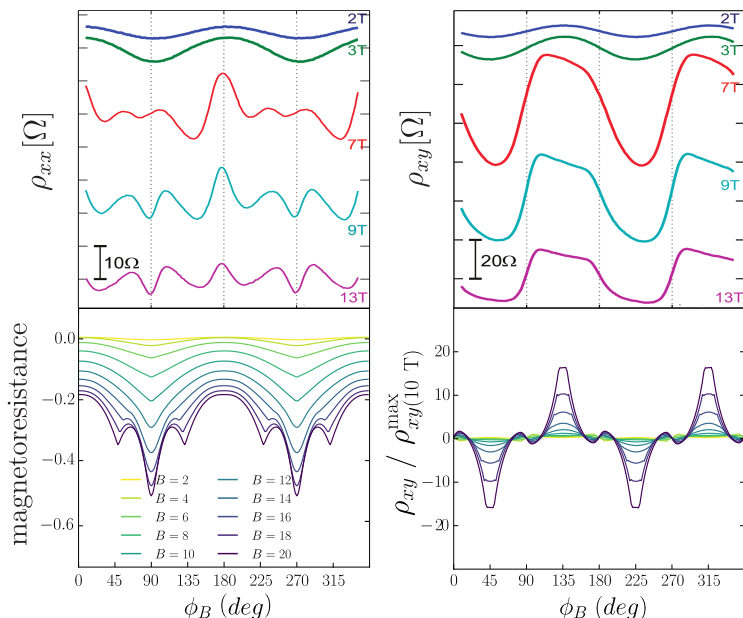


Figure 1.9: (Top) Experimental measurements of the longitudinal (ρ_{xx}) and Hall (ρ_{xy}) resistivity of a Hall-bar device patterned at the LAO/STO interface, as a function of the angle ϕ_B between the current and an in-plane magnetic field. The chemical potential is presumably above the Lifshitz point. Reprinted with permission from A. Joshua, J. Ruhman, S. Pecker, E. Altman and S. Ilani, *Gate-tunable polarized phase of two-dimensional electrons at the $\text{LaAlO}_3 / \text{SrTiO}_3$ interface*, Proc. Natl Acad. Sci., **110**, 9633 (2013). (Bottom) Theoretical calculations of the in-plane magnetoresistance and Hall resistivity (renormalized by the maximum at $B = 10$ T), from Ref. [80]. (These quantities have same angular modulations as ρ_{xx} and ρ_{xy} respectively.)

the metal contact at energy lower than the superconducting gap can be reflected by the interface as a hole, with an additional Cooper pair transferred to the superconductor. This process, called *Andreev reflection*, converts a dissipative current into a (dissipationless) supercurrent.

In the specific case of the interface between a Weyl semimetal in the normal state (N) and a superconductor (S) that pairs electrons at $\pm K$, Andreev reflection must involve a switch of chirality, otherwise it is blocked as long as inversion symmetry is preserved and the internal magnetization of the Weyl semimetal lies in the plane parallel to the NS interface.

The blockade requires the combination of conical dispersion of the Weyl semimetal and spin-momentum locking, thereby it is not a general property of materials with relativistic dispersions. A Zeeman field at the interface

or breaking inversion symmetry can activate Andreev reflection.

1.5.3 Chapter 4

The spectrum of a Weyl semimetal confined to a slab-geometry has a gap for the bulk states, while the dispersion of the surface states is insensitive to the spatial confinement as long as there is no overlap between states on opposite surfaces. Therefore, at energies close to the Weyl points of the unbounded system electrons in the slab have hybrid surface/bulk character depending on the momentum.

The Fermi surface of a conventional two-dimensional electron gas is equivalent to a circle, up to smooth deformations that preserve the orientation of the equi-energy contour. Instead, we show in this chapter that a thin-film magnetic Weyl semimetal with additionally broken inversion symmetry can have a topologically distinct two-dimensional Fermi surface, twisted into a figure-8 — opposite orientations are coupled at a crossing which is protected up to an exponentially small gap due to overlap between wave-functions localized at opposite surfaces.

The topology of the Fermi surface can be probed via quantum oscillations of magnetization (De Haas–Van Alphen effect) or conductance (Shubnikov–De Haas effect) in the presence of an external magnetic field. The frequencies and phase shifts of the oscillations can be extracted from the semiclassical Landau levels, that for this particular system we have computed numerically.

The spectral response of the twisted Fermi surface is distinct from that of a deformed Fermi circle, because the two lobes of a figure-8 cyclotron orbit give opposite contributions to the Aharonov-Bohm phase acquired by the electron wave-function when completing a full orbit. In a strong magnetic field, two counter-propagating types of quantum Hall edge channels appear at the boundaries, when the system is further confined to a strip. However, when an electrical current is driven through the system between two metal reservoirs, only one of the two co-propagating channels is populated, providing unique magnetotransport signatures. For instance, the edge along which the current propagates can be changed by reversing the direction of the magnetic field.

1.5.4 Chapter 5

The work of this chapter was motivated by one of the main results of Chapter 4, that is the value of the phase offset $\gamma = \pi$ obtained as the quantum correction to the semiclassical quantization condition applied to

the figure-8 cyclotron orbit in a thin-film Weyl semimetal. This value of the phase offset differs from the value $\gamma = 0$ offset found for a different type of figure-8 cyclotron orbit, as the energy of the Weyl point in a type-II Weyl semimetal [81].

This apparent inconsistency and the increasing interest in identifying topological semimetals in quantum-oscillation experiments, require a better understanding of how the phase shift encodes information about the topological features of the band structure.

Here we predict the characteristic parameter dependence of the phase shift for Weyl fermions with tilted and overtilted dispersion (type-I and type-II Weyl fermions) and an arbitrary topological charge, including elliptical and 8-shaped Fermi surfaces. Remarkably, for type-II Weyl fermions the phase shift only depends on the quantized topological charge, being insensitive to the specifics of the band structure.

